FINITE ELEMENT MODELLING OF PELLET-CLAD INTERACTION DURING OPERATIONAL TRANSIENTS

T.A. HAYNES, M.R. WENMAN
Department of Materials and Centre for Nuclear Engineering, Imperial College London
Royal School of Mines, Exhibition Road, London, SW7 2AZ – UK

J.A. BALL, J.H. SHEA
Nuclear Technology Branch, EDF Energy
Barnett Way, Barnwood, Gloucester, GL4 3RS – UK

ABSTRACT

A finite element model of pellet-clad interaction in advanced gas cooled reactor fuel experiencing extended reduced power operations is presented. The model considers a 1/8th segment of fuel and overlaying cladding bonded to it. A radial crack is introduced to the pellet, this is able to open and close, straining a section of cladding above the crack. In addition, circumferential cracks in the fuel pellet result in a sliver of fuel being bonded to the cladding; this sliver of fuel contains hairline radial cracks, known as ladder cracks, the opening and closing of which are modelled. Finally, the model predicts the creep strain at the tip of an incipient crack in the cladding, ahead of the radial crack in the fuel pellet. Results show that the crack tip creep strain is strongly dependent on the model of ladder cracking chosen.

1 Introduction

PELICAN is a finite element model, currently under development by Imperial College London, of pellet-clad-interaction at the mid-pellet *r-Θ* plane in advanced gas cooled reactor (AGR) fuel. The model is built in Abaqus 6.11 and makes use of a number of subroutines to replicate many aspects of contemporary fuel performance codes. The model considers a piece of cladding with a sliver of fuel bonded to it. Microscale hairline radial cracks known as 'ladder cracks' pass through the sliver and the remainder of the annular fuel pellet is free to move underneath the clad-sliver composite. Short incipient cracks have been observed in the inner bore of the cladding of a number of different reactors systems[1, 2]; in an AGR, they tend to be seen ahead of radial fuel cracks which pass through both the pellet and sliver. In an AGR, these cracks can grow into the cladding and start longer inter-granular cracks known as clad bore cracks (CBCs). Fig.1a gives an over-view of features observed in AGR post irradiation examination (PIE) and Fig. 1b a summary of the PELICAN model.

Previous development [3] used the radial displacement from EDF Energy's ENIGMA fuel performance code to account for the radial motion of the inner portion of the pellet and the radial power profile in the fuel; the work noted the importance of the competing effects of irradiation creep in the inner regions of the pellet and thermal creep in the cladding. In order to extend PELCIAN to model the complete pellet and to enable the consideration of azimuthal temperature or power profiles resulting from for example, carbon deposition on one side of the fuel pin, the following changes have been made:

- Volumetric strain has been introduced to the fuel; this takes into account sintering, gaseous fission product swelling and solid fission product swelling.
- Thermal conductivity of the uranium dioxide is described by one of three models: Lucuta (1996) [4]; White (1989) [5] and Palmer (2015) [6].
- The radial power profile is accounted for by an implementation of Palmer's RADAR model [7].

- The closure of the ladder cracks was modelled by multiplying the un-cracked elastic modulus of UO_2 by 1.00 when the normalised hoop strain in the sliver is compressive and 0.03 when greater than the fracture strain of UO_2. The normalised hoop strain used is a weighted average (equation (27)) of the elastic hoop strain at integration points in the sliver and within a horizon of the integration point.

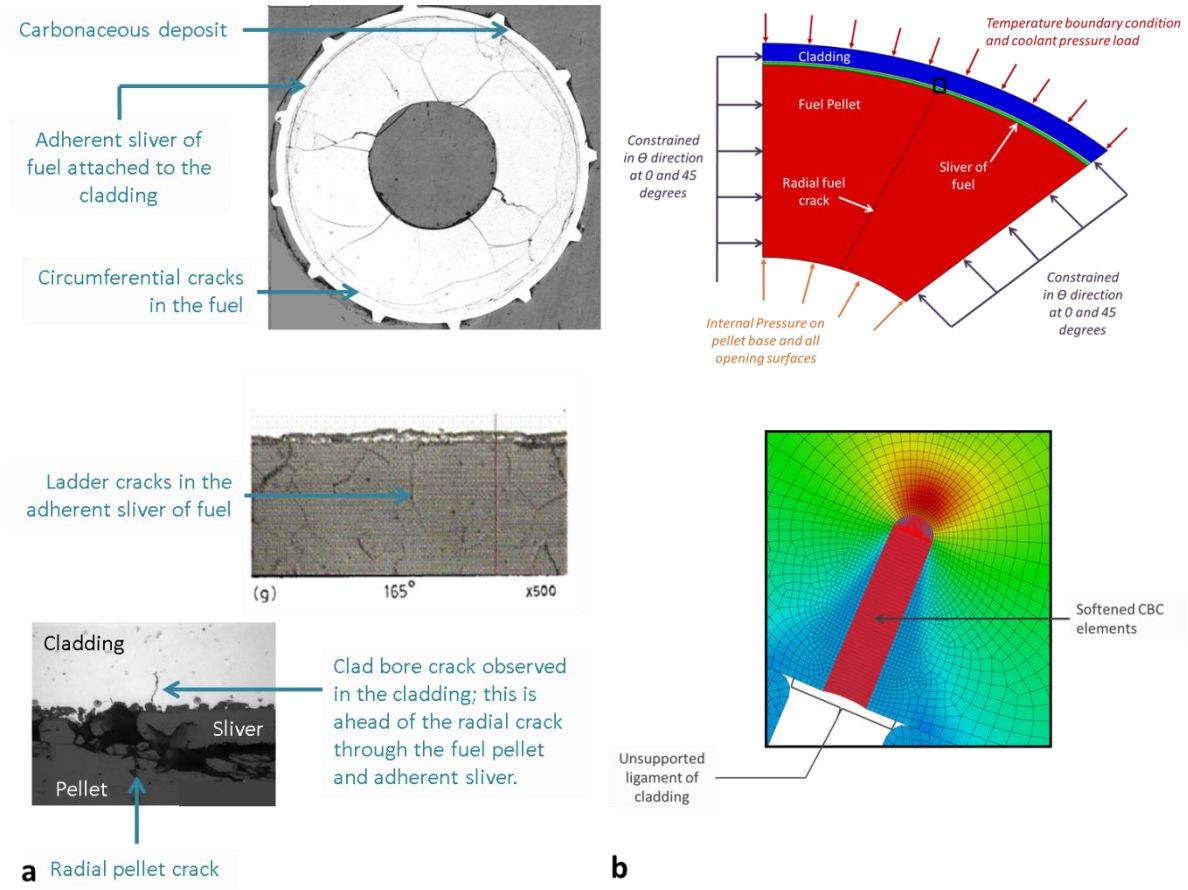

Fig. 1a - A summary of the features of interest in AGR PCI, Micrographs courtesy of EDF Energy Generation.
Fig. 1b – An overview of the PELICAN finite element model of AGR PCI.

2. Methodology

2.1 Volumetric strain

The increment of volumetric swelling strain, $\Delta\varepsilon_{SW}$, was introduced through the creep subroutine and is equal to equation (1). For brevity, we have excluded units and the values used, please refer to the relevant reference. The three terms in the numerator in (1) represent increments of solid fission product swelling, gaseous fission product swelling and irradiation densification; V is the current volume and V_o, the initial volume; Abaqus uses true strain whilst the models use engineering strain.

$$\Delta\varepsilon_{SW} = \frac{\Delta V_{TOTAL}}{V} = \frac{\left(\frac{\Delta V}{V_0}\right)_{TOT}}{\frac{V}{V_0}} = \frac{\left(\frac{\Delta V}{V_0}\right)_{SFP} + \left(\frac{\Delta V}{V_0}\right)_{GFP} + \left(\frac{\Delta V}{V_0}\right)_{IRD}}{\exp(\varepsilon_{SW})} \quad (1)$$

The increment of solid fission product swelling strain, taken from MAPRO section 2.9.2 [8], is given in equation (2); it is a function of the initial density, ρ_0, and the increment of burn-up, ΔBU.

$$\left(\frac{\Delta V}{V_0}\right)_{SFP} = (\Delta\varepsilon_{SW})_{SFP} = A_1\rho_0\Delta BU \quad (2)$$

The increment of gaseous fission product swelling strain used, taken from MAPRO section 2.9.3 [8], is given in equation (3) and is a function of the initial density, increment of burn-up, and temperature, T:

$$\left(\frac{\Delta V}{V_0}\right)_{GFP} = (\Delta\varepsilon_{SW})_{GFP} = A_2\rho_0\Delta BU(T_1 - T)^{n_1}e^{-Q_1(T_1-T)}e^{-Q_2 BU\rho_0} \qquad 1000\text{K} < T < 2000\text{K} \quad (3)$$

The inclusion of the power term accounts for the formation of fission gas bubbles and tunnels on grain boundaries above 1373 K; the first exponential term accounts for increased swelling due to the formation of macropores above 1573 K; finally, the second exponential accounts for the saturation of fission gas swelling at around 10^{26} fissions m^{-3}. Above 1973 K, columnar grains form and fission gas is released into free volumes, additional fuel swelling does not occur and the volumetric strain is set to zero. Similarly, below 1000K it is assumed that no gaseous fission product swelling occurs.

The model for irradiation densification is that developed by White and is based upon fuel stack elongation measurements carried out at Halden and experiments at the Harwell test reactors [9]. The fractional fuel porosity, p, is partitioned into a proportion, α, which can be sintered at a given temperature, of which a proportion, β, sinters more rapidly. The fraction of the initial porosity, p_0, remaining is given by (4)

$$\frac{p}{p_0} = 1 - \alpha[1 - \beta e^{-Q_4 BU} - (1 - \beta)e^{-Q_5 BU}] \quad (4)$$

The proportion of porosity in each partition is a function (5-6) of temperature and grain-size, G:

$$\alpha = \frac{T - A_3}{A_4 G} \quad (5)$$

$$\beta = \frac{A_5}{\alpha}e^{-Q_6/T} \quad (6)$$

Applying conservation of mass to this process yields equation (7), where ρ and ρ_0 are the current and initial densities respectively:

$$\frac{dV}{V_0} = -\frac{\rho_0 d\rho}{\rho^2} \quad (7)$$

The density is related to the porosity and theoretical density, ρ_{th}, according to (8):

$$\rho = (1 - p)\rho_{th} \quad (8)$$

The change in volume during an increment of time due to irradiation densification is calculated by evaluating (4) at the beginning and end of the increment and using equation (9), where ρ_1 and ρ_2 are the initial and final densities calculated using (8). The constant is found by applying mass conservation to the process and the substitution of equation (8) into (7).

$$\frac{dV}{V_0} = \frac{\rho_0\rho_{th}dp}{\rho^2} \approx \frac{\rho_0\rho_{th}dp}{\rho_1\rho_2}$$

$$\therefore \frac{\Delta V}{V_0} \approx \frac{\rho_0\rho_{th}p_0}{\rho_1\rho_2}\left[\left(\frac{p}{p_0}\right)_{end} - \left(\frac{p}{p_0}\right)_{start}\right] \quad (9)$$

2.2 Thermal conductivity

Thermal conductivity is an important parameter to determine in fuel performance modelling as it affects the thermal expansion, swelling, creep and fission gas release in the fuel; fission gas release is not yet modelled by PELICAN and the pin internal pressure is taken from ENIGMA 5.11 output. Following the approach taken by Fink [10], UO_2 thermal conductivity models incorporated into fuel performance codes give the thermal conductivity, k, as the sum of two terms, accounting for phonon and electronic conductivity, multiplied by a number of correction factors k_i:

$$k = \left(k_{ph} + k_{el}\right)\prod_i k_i \quad (10)$$

The phonon term, k_{ph}, takes the form given in equation (11), where $[Gd]$ is the concentration of gadolinia poison; for Lucuta's model, C_1 and C_2 are set to zero and the burn-up dependence is expressed through a multiplicative constant.

$$k_{ph} = \frac{1}{A+BT+C_1BU+C_2[Gd]} \quad (11)$$

The electronic term, k_{el}, takes the form given in equation (12), with varying expressions for the term $D(T, BU)$ given by equations (13-15):

$$k_{el} = D(T, BU)e^{-Q_1/T} \quad (12)$$

$$D(T, BU)_{White} = D_1 + D_2T + D_3T^{-1} \quad (13)$$

$$D(T, BU)_{Palmer} = D_4T^{-2.5} \quad (14)$$

$$D(T, BU)_{Lucuta} = D_5T^{-2} \quad (15)$$

The first multiplicative term, k_{por}, accounts for porosity. Lucuta considers the total porosity, p, and a shape factor, σ; White considers sinterable porosity, p_{sp}, rim porosity, p_{rp}, fission gas porosity, p_{rp}, and pore-former porosities, p_{pf} separately. The Palmer and White models apply separate indices, N_1-N_5, to various categories of fractional porosity, p_1-p_5, based upon their size and shape, Palmer based upon [11, 12] and White on [5].

$$k_{por,White} = (1-p_1)^{N_1}(1-p_2)^{N_2} \quad (16)$$

$$k_{por,Palmer} = (1-p_3)^{N_3}(1-p_4)^{N_4}(1-p_5)^{N_5} \quad (17)$$

$$k_{por,Lucuta} = \frac{1-p}{1+(\sigma-1)p} \quad (18)$$

The majority of international models correct the thermal conductivity for burn-up through the use of multiplicative factors applied to both the phonon and electronic terms: British models such as White and Palmer take a more mechanistic approach and apply the burn-up correction only to the phonon term. Lucuta uses two multiplicative terms, k_{pfp} and k_{dfp}, to account for dissolved fission products and precipitated solid fission products:

$$k_{dfp} = 1 + \frac{1}{F_1+F_2BU^{-1}}\frac{1}{1+\exp(-F_3T+F_4)} \quad (19)$$

$$k_{pfp} = (F_5BU^{-3.265}+F_6BU^{-0.5}T^{-0.5})\arctan\left(\frac{1}{F_7BU^{-3.265}+F_7BU^{-0.5}T^{-0.5}}\right) \quad (20)$$

Palmer and Lucuta include a term, k_{ird}, for irradiation damage; Palmer assumes that the radiation damage anneals quickly and the expression is used only for fuel in-pile:

$$k_{ird} = 1 - \frac{G_1}{1+\exp(G_2T-G_3)} \quad (21)$$

Finally, Lucuta includes a term, k_{sto}, to account for departures from stoichiometry in failed fuel, of the form UO_{2+x}:

$$k_{sto} = \frac{1}{H_1+H_2x+(H_3-H_4x)T} \quad (22)$$

The final expressions of White's [9, 13], Lucuta's [4] and Palmer's [6, 14] thermal conductivity models are therefore given in equations (23-25); in addition, White's model applies a maximum thermal conductivity at low temperatures.

$$k_{White} = \left(k(BU, [Gd], T)_{ph} + k_{el}\right)k_{por,White} \quad (23)$$

$$k_{Palmer} = \left(k(BU, [Gd], T)_{ph} + k_{el}\right)k_{por,Palmer}k_{ird} \quad (24)$$

$$k_{Lucuta} = \left(k(T)_{ph} + k_{el}\right)k_{por,Lucutta}k_{ird}k_{dfp}k_{pfp}k_{sto} \quad (25)$$

2.3 Radial power profile

Palmer's RADAR model [7] was the first to describe the radial power distribution within a fuel pellet due to neutron transport, thermal plutonium breeding and epithermal resonance capture by ^{238}U. It has subsequently been further tuned against the neutronics code WIMS for both AGR and PWR fuel [15], and it is this tuned version which has been introduced into PELICAN. RADAR includes the isotopes ^{235}U, ^{238}U and ^{239}Pu and has since been extended

to include gadolinia poisons and higher burn-ups (through the introduction of additional plutonium isotopes) to form the NEWRAD model in EDF Energy's ENIGMA 5.13 code. The approach also forms the basis for the TUBRNP model used in TRANSURANUS [16, 17] and the current model used in NNL's ENIGMA-B [18]. As it stands, RADAR is validated for low burn-up (< 30 GWd/tU) AGR and LWR fuel and so is appropriate to PELICAN.

2.4 Ladder cracks

Work by Mella and Wenman [19] has shown that fuel pellets are likely to experience considerable damage on their outer surface during the initial rise to power; the current version of PELCIAN therefore assumes that ladder cracks can form at any part of the fuels life. In addition, ladder cracks are rarely observed in routine PIE since some major radial cracks (extending the full radius of the pellet) have been observed to close and possibly heal [20]. It is therefore assumed that once the ladder cracks close, the elastic modulus of the fuel returns to the un-damaged value. PELICAN adopts the model for the elastic modulus of the sliver, E, given in (26) where E_0 is the undamaged elastic modulus; ε_{NL}, the non-local hoop strain given by equation (27) and ε_f, the fracture strain of UO_2. This was assumed to be 5.0x10^{-4} (based upon an elastic modulus of ~ 200 GPa and a fracture stress of 100 MPa [9, 19]. The parameter K_0, has previously been determined by tuning to clad wall thinning strains to be 0.03 [21]:

$$\begin{aligned} E &= E_0 && \varepsilon_{NL} < 0 \\ E &= K_0 E_0 && \varepsilon_{NL} > \varepsilon_f \\ E &= \left(1 - \frac{1-K_0}{\varepsilon_f}\varepsilon_{NL}\right) E_0 && \varepsilon_{NL} > \varepsilon_f \end{aligned} \qquad (26)$$

The non-local hoop strain at element i is determined at each element by multiplying the hoop strain at all other elements j contained within the sliver and a horizon of influence, r_H, by a weighting factor and dividing this by the sum of the weighting factors within the horizon (equation (27)). The weighting factor takes the form of an inverse exponential of distance between the two elements, $r_{i,j}$, divided by a characteristic length, l_c; the horizon was taken as three times the sliver thickness and the characteristic length chosen to be twice the sliver thickness so as to remove the fluctuations. The non-local formulation was introduced to remove mesh-sensitive fluctuations in the elastic modulus between neighbouring elements.

$$\varepsilon_{NL,i} = \frac{\sum_j \varepsilon_{\theta,j} e^{-r_{i,j}/l_c}}{\sum_j e^{-r_{i,j}/l_c}} \qquad (27)$$

2.5 Simulated operating conditions

In order to demonstrate the model, the fuel was run at full power (701.6 ºC and 20.1 kW m^{-1}) for 330 days; the power was reduced to 70% of full power (609.6 ºC and 14.1 kW m^{-1}) over 10 hours; this was followed by a 30 day period of extended reduced power operation and then a return to full power over 10 hours and a further hold at full power for 180 days.

3 Results & Discussion

3.1 Radial power and burn-up profile

The same RADAR model has been implemented into PELICAN as is used as the default for AGR fuel in EDF Energy's ENIGMA 5.13 and the same rating profile is therefore applied to both ENIGMA and PELICAN (Fig. 2a). The burn-up profiles taken from the two models (Fig. 2b) agree to within 1.1%; the slight difference is due to a combination of the use of 12 annular zones in ENIGMA and the calculation of the relative radius from PELICAN.

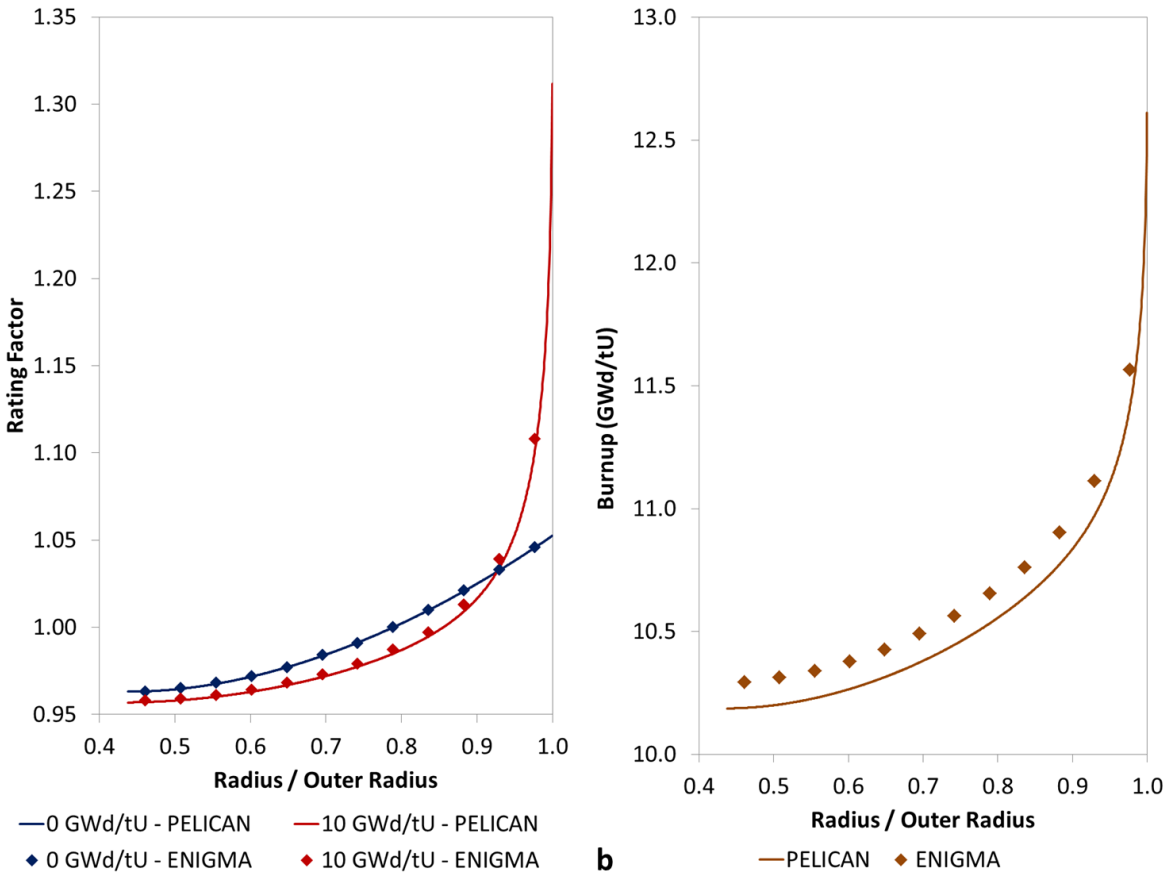

Fig. 2a – Comparison of the radial rating profile against EDF Energy's ENIGMA 5.13 and Fig. 2b – Comparison of the radial burn-up against EDF Energy's ENIGMA 5.13.

3.1 Thermal conductivity

Fig. 3a shows the radial temperature through the fuel at the end of the simulation (9.0 GWd/tU) and Fig. 3b the pellet bore temperature during a simulation in which the reduction to 70% did not take place. Generally, using Lucuta's model results in a pellet bore temperature around 40 ºC lower than using either Palmer or White's model. It should be remembered that Palmer and White made use of similar datasets for the temperature dependence, Palmer used Halden data for the burn-up trend White made use of Riso data. The pellet bore temperature increases with burn-up due to the degradation of thermal conductivity; using Lucuta's model, the temperature increase becomes noticeable after around one year (≈ 7 GWd/tU), the decrease in temperature early in life is due to pellet densification. Palmer's model gives a slightly slower degradation in thermal conductivity than White's. Comparing the implementation of White's model into ENIGMA and PELCIAN, the variation of temperature with position in the pellet and burn-up is near identical; the slight offset of 5 ºC is due to the more simple clad-fuel thermal conductivity model used in PELICAN. It should be noted the current version of PELICAN does not include the build up of fission gas porosity and this explains the linear trend of centreline temperature with burn-up demonstrated in Fig. 3b.

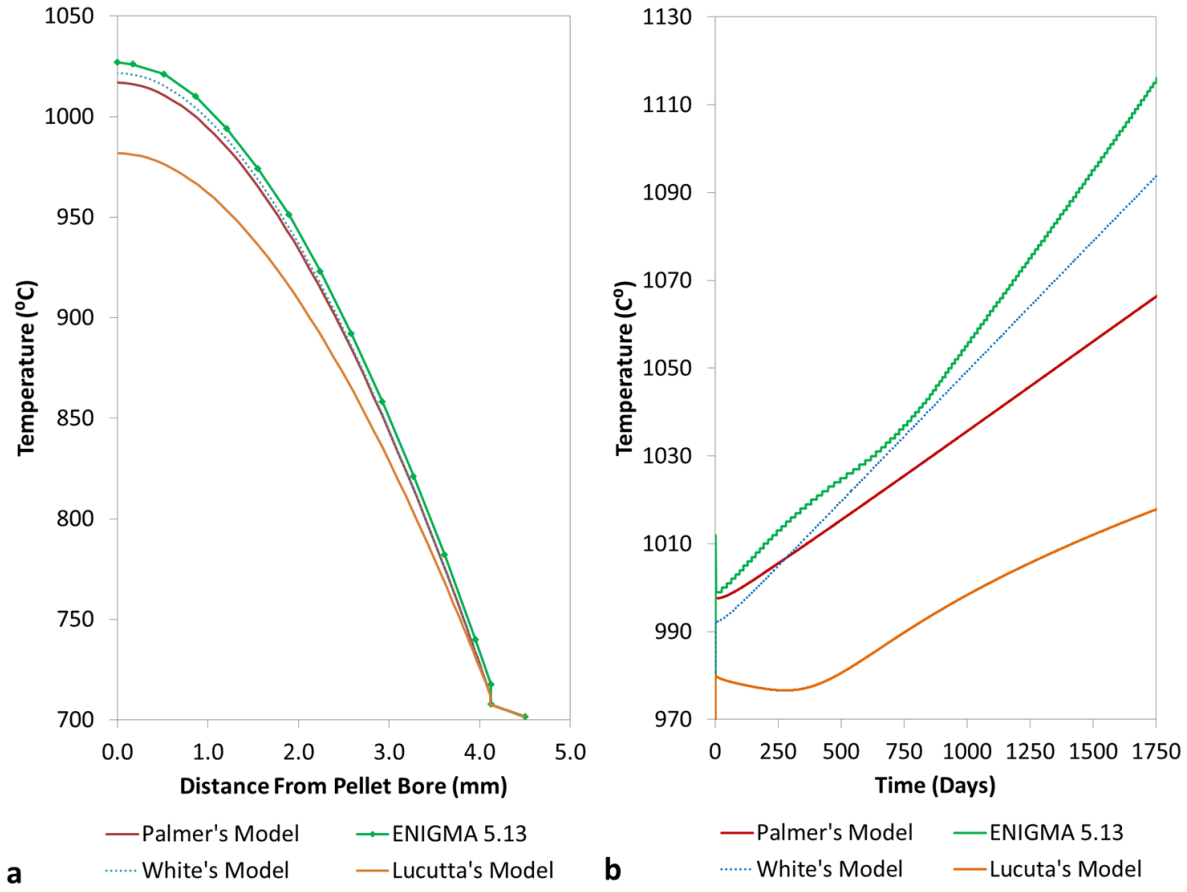

Fig. 3a - Radial profile of temperature at the end of the simulation and
Fig. 3b – Pellet bore temperature during the simulation.

3.3 Pellet relocation

Fig. 4 shows the displacement of the outer surface of the fuel pellet and the opening and closing of the radial crack at its tip and base during the transient. Fig. 4 shows that during the down-rate, both the pellet bore and pellet outer surface move inwards, the outer surface moving more due to the decreased temperature drop across the fuel. In addition, the base of the pellet crack opens whilst the top closes. Due to irradiation creep during the low power hold (10 - 730 h), the pellet bore closes further, the base of the crack closes more and the crack tip opens more. During the up-rate, the base of the crack shuts, the tip opens and the bore and outer surface are displaced outwards. Following the period of low power operation, the pellet crack has opened more at the inner surface and the point of contact between the fragments has moved inwards, the bore is smaller and the outer surface has moved inwards. This retreat of the pellet outer displacement is in marked contrast to earlier results from PELICAN [3] and is due to increased creep into the pellet bore during the hold at low power and the modelling of pellet relocation along the pellet crack.

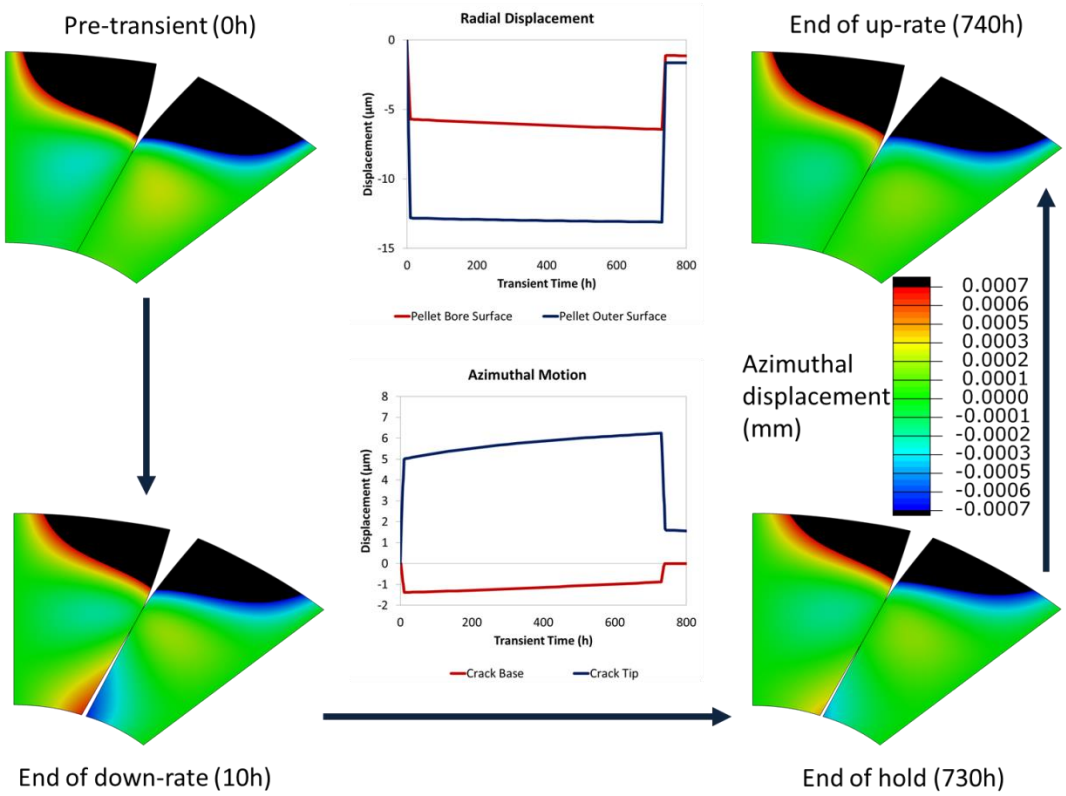

Fig. 4 - Azimuthal and radial relocation of the fuel pellet during low power operation. The shape of the azimuthal displacement of the fuel pellets fragments has increased by a factor of 1000 to aid clarity.

3.4 Ladder crack closure

Fig. 5a compares the creep strain accrued at the CBC tip in models in which ladder cracks are always open, always closed and able to open and close. Enabling the cracks to open and close gives a creep strain between that accrued with permanently open and permanently closed ladder cracks. The slow expansion of the pellet and the opening of the pellet crack during steady state operation at full power causes the ladder cracks surrounding the CBC to be closed and those some distance away to be open (Fig. 5b). The creep strain accrued at the CBC prior to the transient therefore matches the permanently closed model (Fig. 5a). During the initial part of the down-rate, a front of ladder crack closure slowly advances away from the radial pellet crack; around 7h into the 10h down-rate, the ladder cracks in the rest of the sliver start to close and by the end of the down rate they are all closed. The closure of the ladder cracks during the latter part of the down-rate increases the hoop stress at the CBC and the creep strain accrued at the CBC compared to the model in which ladder crack closure is not modelled. Modelling the closure of the ladder cracks is clearly important as ladder crack closure during the down-rate increased the creep strain accrued at the CBC tip and this has been observed in previous work [3] to be a good predictor of the overall trend in CBC depth with fuel element number.

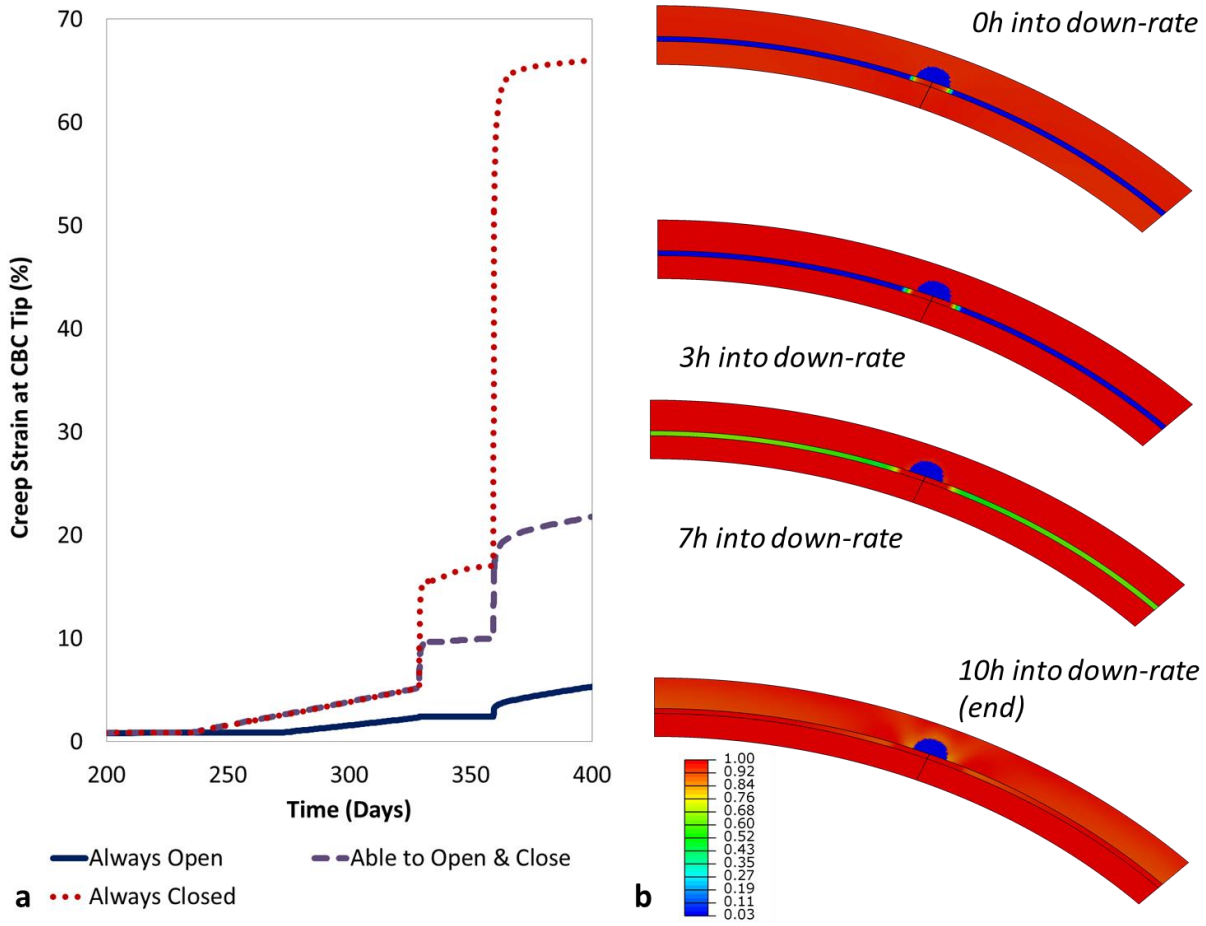

Fig. 5a - The equivalent creep strain accrued at the CBC tip for models in which ladder cracks are always open, always closed and able to open and close.

Fig. 5b – Ladder crack closure during the down-rate. Red areas are those in which the ladder cracks are closed and blue areas in which they are open. Green regions show regions where the ladder cracks are in the process of cracking.

4 Conclusions

- During down-rates, pellet cracks are shown to close at their tip and open at their base.
- Further crack closure and pellet relocation, driven by irradiation creep at reduced power, causes pellet bore closure and reduced radial displacement of the fuel pellet.
- During steady state operation at the power and temperature level modelled, the ladder cracks surrounding the radial pellet crack and associated CBC are closed whilst those some distance away are open.
- Around half-way through a down-rate, the remainder of the ladder cracks close. This is associated with an increased accrual at of creep strain at the CBC compared to the model in which the ladder cracks do not close.

5 Future Work

Future work will take the model in a number directions: modelling a cross-pin temperature tilt resulting from a greater thickness carbon deposit on one side of the fuel pin compared to the other; modelling the growth of the clad bore crack within the cladding; and, investigating the behaviour of the major pellet cracks and hairline ladder cracks under a greater range of operating conditions as well as the effect of changing l_c and r_H.

6 Acknowledgments

Thomas Haynes would like to thank Dr I.D. Palmer from the UK's National Nuclear Laborary, Springfield; and, Dr S. Morgan from the UK's National Nuclear Laborary, Windscale. Thomas Haynes and Mark Wenman would like to thank EDF Energy Generation and the Engineering and Physical Sciences Research Council for their financial support.

7 References

1. Lysell, G., et al., Cladding Linear Surface Effects and PCI. Pellet-Clad Interaction in Water Reactor Fuels Transactions, Aisx-en-Provence, 2004: p. 273-278.
2. Kitano, K.L., C., J. Arborelius, and M. Limbäck, Study on incipient cracks at inner surface of cladding liner after high power irradiation test. Water Reactor Fuel Performance Meeting (TopFuel) 2005 Transactions, 2005: p. 268-275.
3. Haynes, T.A., et al., Modelling pellet-clad mechanical interaction during operational transients in bonded nuclear fuel. Journal of Nuclear Materials, 2015. 465: p. 280-292.
4. Lucuta, P.G.M., Hj. and I.J. Hastings, A pragmetic approach to modelling thermal conductivity of irradiated UO_2 fuel : review and recommendations. Journal of Nuclear Materials, 1996. 1996(232).
5. Turnball, J.A.W., R.J., The effect of burn-up on fuel thermal conductivity. Central Electricity Generating Board, 1988. UO2BPC/P(87)230.
6. Palmer, I.D., Uranium Dioxide Properties Data Manual: Data Sheet 3, Thermal Conductivity. EDF Energy, 2015. E/REP/BCBB/0083/GEN/14.
7. Palmer, I.D., K.W. Hesketh, and P.A. Jackson, A Model for Predicting the Radial Power Profile in a Fuel Pin. Water Reactor Fuel Element Performance Computer Modelling, 1983: p. 321-335.
8. Siefken, L.J., et al., MATPRO - A Library of Materials Properties for Light-Water-Reactor Accident Analysis. Idaho National Engineering and Environmental Laboratory, 2001.
9. White, R.J., An analysis of Halden fuel stack length changes and comparison with UK sintering data. Halden Programme Group Meeting, 1990. HPR-336/13.
10. Fink, J.K.C., M.G. and L. Leibowitz, Thermophysical properties of uranium dioxide. Journal of Nuclear Materials, 1981. 102: p. 17-25.
11. Bakker, K. and R.J.M. Konings, The effects of irradiation on the thermal conductivity of high burnup UO_2 fuel. International Atomic Energy Agency, 1996. TECDOC-1036 : Advances in fuel pellet technology for improved performance at high burnup p. 149-160.
12. Ikatsu, N., et al., Influence of rim effect on fuel centre temperature. International Atomic Energy Agency, 1998. TECDOC-1179 : Fuel chemistry and pellet-clad interation related to high burnup fuel(Proceedings of a Technical Committee meeting held in Tokyo, 28 October - 1 November 1996).
13. Shea, J.H., The ENIGMA fuel performance code description: Version 5.14. EDF Energy, 2009. E/REP/BBFB/0039/GEN/07.
14. Palmer, I.D., Review of fuel thermal conductivity recommendations and models. National Nuclear Laboratory, 2012.
15. Palmer, I.D., Personal Communication. 2015.
16. Lassmannm, K., et al., The radial distribution of plutonium in high burnup UO2 fuels. Journal of Nuclear Materials, 1994. 208: p. 223-231.
17. Schubert, A., et al., Extension of the TRANSURANUS burn-up model. Journal of Nuclear Materials, 2008. 376: p. 1-10.
18. Rossiter, G.D., P.M. Cook, and R. Weston, Isotopic modelling using the ENIGMA-B fuel performance code. National Nuclear Laboratory, 2000.
19. Mella, R. and M.R. Wenman, Modelling facture of nuclear fuel pellets during a power transient using peridynamics. In Review : Journal of Nuclear Materials, 2015.
20. Morgan, S., 2015. Personal Communication.
21. Shea, J.H., et al., Modelling the effects of flexible operation on AGR fuel integrity. TopFuel '97 Transactions, 1997. 5: p. 176-183.